ACS central science

Research Article

http://pubs.acs.org/journal/acscii

Facile Synthesis of Uniform Virus-like Mesoporous Silica Nanoparticles for Enhanced Cellular Internalization

Wenxing Wang,[†] Peiyuan Wang,[†] Xueting Tang,[†] Ahmed A. Elzatahry,[‡] Shuwen Wang,[†] Daifallah Al-Dahyan,[§] Mengyao Zhao,[†] Chi Yao,[†] Chin-Te Hung,[†] Xiaohang Zhu,[†] Tiancong Zhao,[†] Xiaomin Li,[†] Fan Zhang,*[,†] and Dongyuan Zhao*[,†]

[†]Department of Chemistry, Collaborative Innovation Center of Chemistry for Energy Materials, State Key Laboratory of Molecular Engineering of Polymers, Fudan University, Shanghai 200433, P. R. China

[‡]Materials Science and Tech Program, College of Arts and Sciences, Qatar University, P.O. Box 2713, Doha, Qatar

[§]Department of Chemistry, King Saud University, Riyadh, 11451, Saudi Arabia

Supporting Information

ABSTRACT: The low-efficiency cellular uptake property of current nanoparticles greatly restricts their application in the biomedical field. Herein, we demonstrate that novel virus-like mesoporous silica nanoparticles can easily be synthesized, showing greatly superior cellular uptake property. The unique virus-like mesoporous silica nanoparticles with a spiky tubular rough surface have been successfully synthesized via a novel single-micelle epitaxial growth approach in a low-concentration-surfactant oil/water biphase system. The virus-like nanoparticles' rough surface morphology results mainly from the mesoporous silica nanotubes spontaneously grown via an epitaxial growth process. The obtained nanoparticles show uniform particle size and excellent monodispersity. The structural parameters of the nanoparticles can be well tuned with controllable core diameter (~60−160 nm), tubular length (~6−70 nm), and outer diameter (~6−10 nm). Thanks to the biomimetic morphology, the virus-like nanoparticles show greatly superior cellular uptake property (invading living cells in large quantities within few minutes, <5 min), unique internalization pathways, and extended blood circulation duration ($t_{1/2}$ = 2.16 h), which is much longer than that of conventional mesoporous silica nanoparticles (0.45 h). Furthermore, our epitaxial growth strategy can be applied to fabricate various virus-like mesoporous core−shell structures, paving the way toward designed synthesis of virus-like nanocomposites for biomedicine applications.

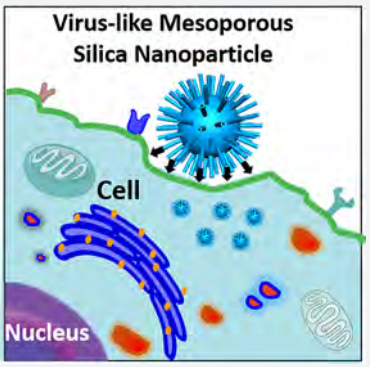

Nowadays, multifarious nanoparticles have been designed for biomedical applications such as intracellular drug delivery and molecular imaging.[1−9] Their efficiency heavily relies on the cellular uptake performance.[10−16] The interaction between nanoparticles and biological hosts (e.g., HeLa cell, *Escherichia coli*) plays an important role in the cellular uptake process, which is greatly dependent on the chemical and physical properties of the nanoparticles.[17,18] Previous reports have introduced various methods to enhance the cellular uptake property by controlling factors that could influence the interaction between nanomaterials and biological hosts, such as chemical composition, particle shape, and surface charge.[19−29] However, studies on regulating the interaction between nanomaterials and biological hosts by improving the surface topological structures of nanomaterials are relatively rare.[10,30,31]

Some viruses have been demonstrated to have good cellular invasion properties owing to their rough surface consisting of spike proteins, which can bind strongly to cell membranes during the invasion process.[32,33] Inspired by the unique surface morphology of virus, several recent works have been carried out to fabricate nanomaterials with the topological structures of viruses.[10,34] Unfortunately, their tedious and uncontrollable synthetic processes as well as their unfavorable aggregation and poor porosity greatly limit their further applications in biomedicine such as intracellular drug delivery. It is of great importance and a challenge to develop a facile approach to precisely fabricate well-controlled virus-like nanoparticles with excellent monodispersity and open large channels, so as to meet the requirements of efficient cellular uptake in various biological applications. To date, virus-like-structured porous particles with perpendicular spiky nanotubes have never been reported yet. Furthermore, no feasible method has been developed to realize the fabrication of a virus-mimetic surface structure with large mesopore channels on various substrates of diverse composition, size, and shape.

In the present work, uniform virus-like mesoporous silica nanoparticles with inner mesoporous nanospheres surrounded by epitaxial perpendicular mesopore nanotubes have successfully been synthesized for the first time via a novel single-micelle epitaxial growth approach in a low-surfactant-concen-

Received: June 18, 2017
Published: July 26, 2017

DOI: 10.1021/acscentsci.7b00257
ACS Cent. Sci. 2017, 3, 839−846

tration oil/water biphase reaction system, using hexadecyltrimethylammonium bromide (CTAB) as a structural template and tetraethyl orthosilicate (TEOS) as a precursor. The unique monodispersed virus-like mesoporous silica nanoparticles show a very uniform particle size, well-controllable mesoporous nanotube length and inner diameter. These separate nanotubes grow radially from the inner mesoporous silica nanospheres, forming a rough surface structure similar to the spike proteins of viruses. Ascribed to the virus-like rough surface, the obtained mesoporous silica nanoparticles can invade living cells in large quantities within 5 min, displaying the fastest cellular uptake rate. In addition, it is interesting to find that the virus-like mesoporous silica nanoparticles show unique internalization pathways and an extended blood circulation duration ($t_{1/2}$ = 2.16 h), which is significantly longer than that of conventional mesoporous silica nanoparticles (0.45 h). The virus-like nanoparticles loaded with doxorubicin (DOX) show much higher cancer cell toxicity, suggesting great potential for biological applications. Moreover, our strategy can be further extended to fabricate functional nanoparticles@virus-like mesoporous silica core−shell composite structures with tunable structural parameters. It paves the way for designed synthesis of various virus-like functional core−shell nanocomposites.

Uniform virus-like mesoporous silica nanoparticles can be synthesized in a biphase reaction system with a low surfactant concentration, which allows the coassembly of reactants to take place at the oil−water interface for continuous interfacial growth. The oil phase was adopted in the upper of the beaker to be a TEOS solution in hydrophobic organic solvent (such as cyclohexane), while the bottom water phase was an aqueous solution of cationic surfactant (CTAB) as a template and NaOH as a catalyst. Scanning electron microscopy (SEM) and transmission electron microscopy (TEM) images of the obtained mesoporous silica nanoparticles clearly show a unique virus-like morphology with uniform particle size of ∼160 nm (Figure 1). Each virus-like mesoporous silica nanoparticle is composed of two parts with different geometrical structures: (i) interior spherical mesoporous silica cores with a diameter of ∼110 nm; (ii) separated peripheral silica nanotubes perpendicular to the core surface with a length of ∼35 nm and outside/inside diameters of 10/2.5 nm, respectively (Figures 1 and S1). The size of the mesoporous silica cores can be tuned from ∼60 to 160 nm by changing feeding amount of the surfactant (CTAB). The length of the mesoporous silica nanotubes can also be well tuned from ∼6 to 70 nm by simply controlling the time length for epitaxial growth. The obtained virus-like mesoporous silica nanoparticles have a high surface area of ∼289−568 m^2/g (Figures S2−S4). The pore size distribution calculated with the nonlocal density functional theory (NLDFT) method shows that the silica nanoparticles have a uniform mesopore size of ∼2.5 nm (Figure S2), consistent with the inner diameter of the silica nanotubes. The distance between two adjacent silica nanotubes is about 30 nm (Figure 1b,d), suggesting that only a few mesopore channels can grow to form the long separated nanotubes. The spaces between the silica nanotubes also dedicate some mesopore volumes, which has a good agreement with the pore size distribution results from 30 to 60 nm as shown in Figure S2. The small-angle X-ray scattering (SAXS) pattern of the virus-like mesoporous silica nanoparticles shows two scattering peaks at 0.25 and 0.81 nm^{-1} (Figure S5), which can be attributed to the spacing between adjacent nanotubes and interior mesoporous silica spherical cores, respectively.

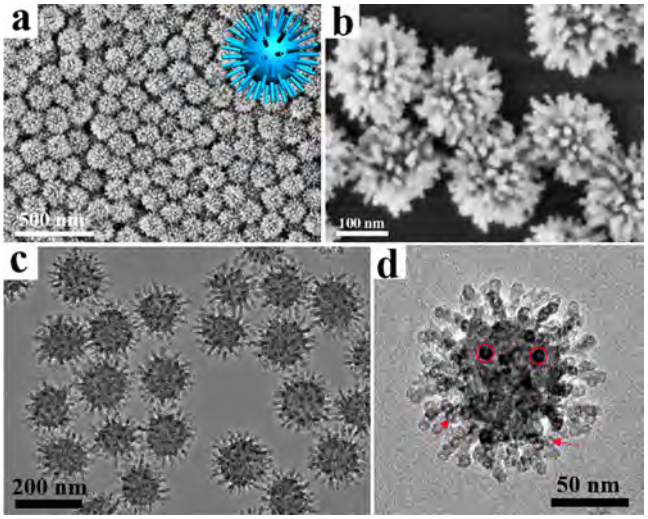

Figure 1. Structural characterization of virus-like mesoporous silica nanoparticles. (a, b) SEM and (c, d) TEM images with different magnifications of the virus-like mesoporous silica nanoparticles. The red arrows mark the open tubular structures, and the red circles highlight the top view of the open silica nanotubes. The inset of (a) is the structural model for the virus-like mesoporous silica.

TEM and SEM measurements were employed to investigate the formation process of the virus-like mesoporous silica nanoparticles (Figures 2 and S6). Mesoporous silica nanoparticles with a diameter of ∼50 nm, pore size of ∼5.3 nm, and pore wall thickness of ∼2 nm can be obtained in the low-surfactant concentration system after a growth process for 6 h (Figures 2a and S7). The Brunauer, Emmett, and Teller (BET) surface area of the product was calculated to be ∼467 m^2/g (Figure S7). A single scattering peak was observed in the SAXS pattern at ∼0.87 nm^{-1}, which could be assigned to the uniform mesostructure of the silica nanospheres (Figure S8). After a reaction for 12 h, the diameter and mesopore wall thickness of the silica nanoparticles increased to ∼80 and ∼3.5 nm, respectively. The BET surface area and pore size decreased to ∼256 m^2/g and ∼4.8 nm, respectively (Figure S7). As shown in the SAXS pattern, the scattering peak was at the same position (Figure S8). As the reaction time was further prolonged, the mesoporous silica particles grew up to ∼100 nm, and the mesopore walls became thicker and thicker. Correspondingly, the BET surface area reduced to ∼89 m^2/g (Figure S7) after 18 h, implying that some of mesopore channels were blocked and covered caused by further growth of excessive silicates with insufficient surfactant template. After reacting for 24 h, short silica nanotubes started to form separately on the surface of the nanoparticles (Figure 2d). No obvious change was detected in particle size and BET surface area (Figures 2d and S7). With the reaction going on, the silica nanotubes grew longer to ∼5 nm, and the particle size increased to ∼130 nm. Meanwhile, the BET surface area also increased to ∼112 m^2/g (Figures 2e and S7). Finally, the length of the nanotubes grew to ∼15 nm and the particle size of the mesoporous silica spherical cores increased to ∼160 nm after 48 h (Figure 2f). The BET surface area increased to ∼190 m^2/g (Figure S7), which could be attributed to the elongation of the nanotubes. After the hydrothermal treatment at 100 °C, the surface area increased to ∼568 m^2/g, which is a comparable value with conventional mesoporous silica nanoparticles, and the morphology was well

DOI: 10.1021/acscentsci.7b00257
ACS Cent. Sci. 2017, 3, 839−846

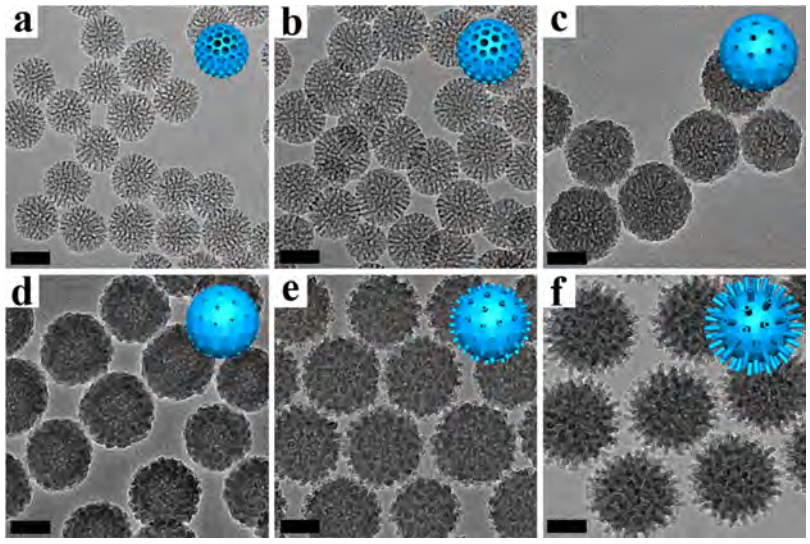

Figure 2. Formation process of virus-like mesoporous silica nanoparticles. TEM images of the mesoporous silica nanoparticles prepared at different reaction times: (a) 6 h; (b) 12 h; (c) 18 h; (d) 24 h; (e) 36 h; (f) 48 h, respectively, in a biphase (cyclohexane and water) reaction system with a low CTAB-surfactant concentration. The insets are the structural models for the mesoporous silica nanoparticles. All the scale bars are 50 nm.

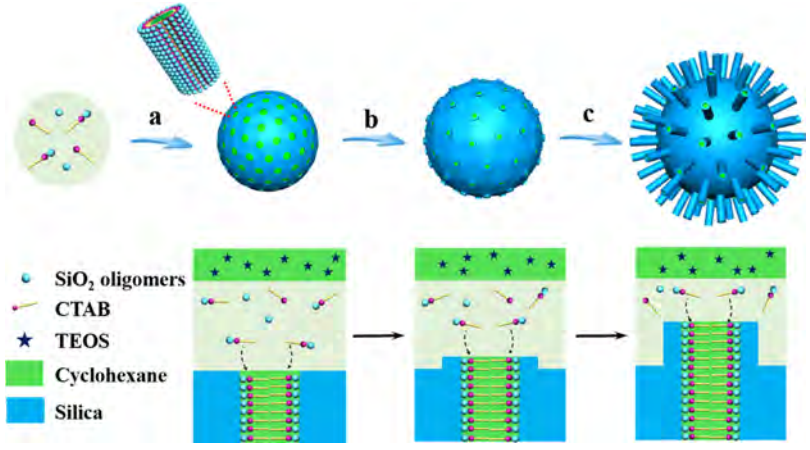

Figure 3. Schematic illustration of the formation process. (a) Formation and growth of mesoporous silica nanoparticles. (b) Formation of the nucleation sites. (c) Orientated growth of the silica nanotubes.

retained (Figures S3 and S4). The SAXS patterns (Figure S8) of the mesoporous silica nanoparticles obtained after different reaction times showed the same scattering peaks at ∼0.87 nm^{-1}, indicating uniform interior mesostructures of same cell parameters. Meanwhile, a new scattering peak could be observed at 0.53 nm^{-1} in the SAXS pattern of the virus-like particles obtained after 48 h reaction, which could be assigned to the mesoscopic distribution of the peripheral perpendicular silica nanotubes. Furthermore, the growth process indicated that the length of the silica nanotubes could be well tuned from ∼6 to 70 nm by controlling the reaction time (Figure S9).

During the reaction process, the formation of the virus-like mesoporous silica nanoparticles could be affected by the concentration of surfactants and species of the oil phase. First, the concentration of surfactants could influence the size of the silica spherical cores (Figure S10). As shown in Figure S11, the core diameters of the mesoporous silica particles were measured to be ∼106, 131, and 156 nm when the surfactant concentration increased from 2.0, to 3.0, and 4.0%, respectively. Second, three kinds of organic reagents including 1-octadecene, decahydronaphthalene, and cyclohexane were used as the oil phase to prepare the virus-like mesoporous silica nanoparticles, and all three samples possessed spiky nanotubes with different lengths. As shown in Figure S12, the lengths of the nanotubes were measured to be ∼8, 12, and 20 nm when 1-octadecene, decahydronaphthalene, and cyclohexane was used as an oil phase, respectively. To further understand the effect of the oil phase, the silica precursor TEOS was directly added into the reaction system without any oil solvent. The mesoporous silica nanoparticles with short nanotubes of ∼6 nm were obtained, showing a similar length with those synthesized in the 1-octadecene system (Figure S13). Meanwhile, the outer diameter of the silica nanotubes obtained in the absence of oil phase was small (∼6 nm).

As mentioned above, the inner diameter of the silica nanotubes on the surface is ∼2.5 nm (Figure S1), very consistent with the size of the CTAB cylindrical single micelle. It implies that each silica nanotube is templated by cylinder single micelles.[35,36] The SEM image shows distinct short nanotubes distributed separately on the surface of the silica nanoparticles obtained after reacting for 21 h. And finally, virus-like mesoporous silica nanoparticles with long nanotubes could

DOI: 10.1021/acscentsci.7b00257
ACS Cent. Sci. 2017, 3, 839−846

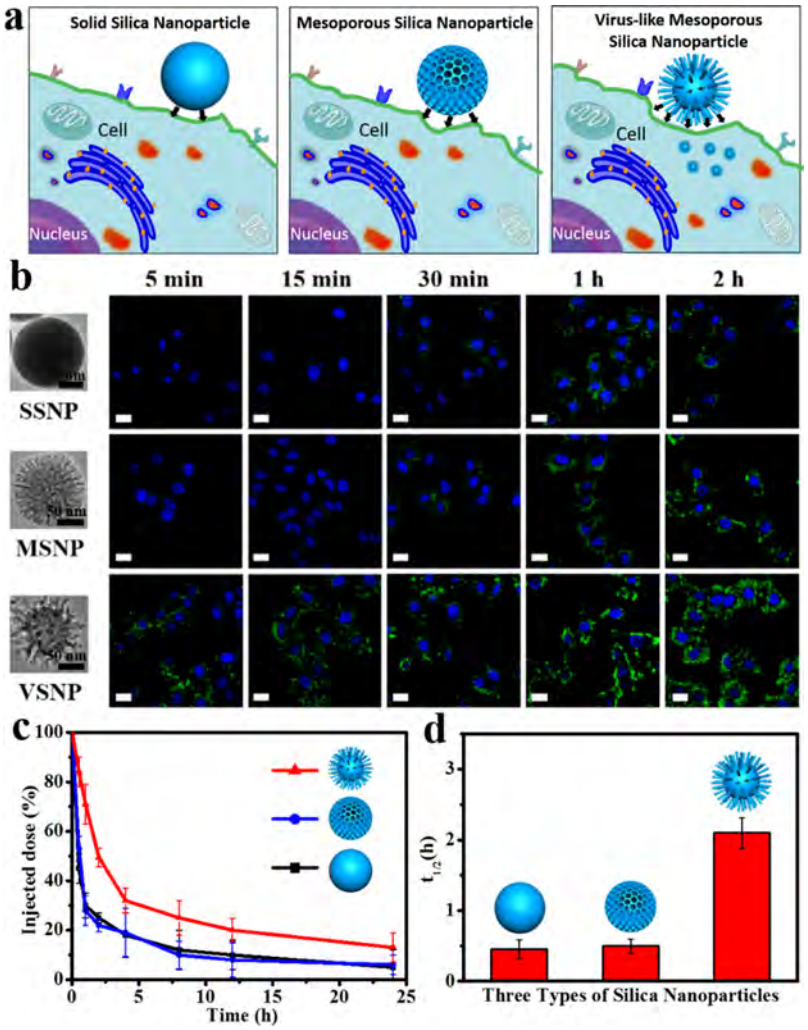

Figure 4. Cellular internalization and in vivo blood circulation. (a) Schematic illustration for cellular uptake of three types of silica nanoparticles. (b) Confocal laser scanning microscopy (CLSM) observations of the HeLa cells after incubation with the solid silica nanoparticles (SSNPs), conventional mesoporous silica nanoparticles (MSNPs), and the virus-like mesoporous silica nanoparticles (VSNPs) for 5 min, 15 min, 30 min, 1 and 2 h. (c) Time-dependent blood level upon tail vein injection of three types of nanoparticles, calculated as percentage of injected dose remaining in the blood. (d) Blood circulation half-lives ($t_{1/2}$) of three types of nanoparticles. Error bars were based on three mice per group at each time point and three repetitions, $P < 0.05$. All the scale bars are 10 μm.

be obtained (Figure S14). This result clearly indicates that the orientated growth of the mesoporous silica nanotubes takes place assisted by the single micelles (Figure S15).

On the basis of the results above, we propose that single-micelle templating epitaxial growth induced by an ultralow surfactant concentration occurred during the formation of the uniform virus-like mesoporous silica nanoparticles (Figure 3). The formation process of the virus-like silica nanoparticles experiences an isotropic growth of the spherical mesoporous silica nanoparticles under an ultralow concentration of surfactant template followed by an orientated growth of the silica nanotubes from the mesopore channels. It mainly involves three stages, i.e., (i) the formation of mesoporous silica spherical nanoparticles; (ii) the formation of nucleation sites on the surface of the mesoporous silica nanoparticles and the necks of the mesopore channels; (iii) single-micelle epitaxial growth of the silica nanotubes on the surface and necks of the mesoporous silica nanoparticles. First, the silica precursor (TEOS) in the upper organic solvent diffuses into the aqueous phase gradually to form the mesoporous silica spherical nanoparticles at the interface of oil/water biphase as reported previously.[37,38] The mesoporous silica spherical nanoparticles grow larger with prolongation of reaction time, while the concentration of the surfactant and silicate oligomers decreases gradually.[38] With further consumption of the reactants, the surfactants and silicate oligomers in aqueous phase become insufficient for the isotropic growth of the mesoporous silica nanoparticles. As a result, some of the mesopore channels get covered and blocked, resulting in closed mesopores, which can be reopened after a hydrothermal treatment. At the same time, some of the silicate oligomers are deposited partially on the surface of the silica nanospheres and necks of mesopore channels, functioning as nucleation sites for further growth into perpendicular nanotubes. It is fair to assume that the deposition tends to take place along some of the mesopore channels of the previously formed mesoporous nanospheres because the micelles already exist because of the hydrophilic−hydrophobic interaction. As a result, the single-micelle induced epitaxial growth leads to the formation of separated nanotubes on the surface and mesochannel necks of spherical silica nanoparticles. With further growth of the nanotubes induced by cylinder

DOI: 10.1021/acscentsci.7b00257
ACS Cent. Sci. 2017, 3, 839−846

single micelles, uniform virus-like mesoporous silica nanoparticles can be obtained.

In general, nanomaterials should be designed to enter cells rapidly and efficiently to realize a better therapeutic effect.[17] Here, cell internalization of three types of FITC-labeled nanoparticles (Figure S16), solid silica nanoparticles, conventional mesoporous silica nanoparticles, and virus-like mesoporous silica nanoparticles, were examined against HeLa cells (Figure 4a,b). It was found that the relative uptake rate was quite different for each type of nanostructure. After incubation for 5 min, the virus-like mesoporous silica nanoparticles obtained above could penetrate the cellular membrane and accumulate throughout the cytosol. While for the solid silica nanoparticles and conventional mesoporous silica nanoparticles, luminescence signals were not detected at all inside the cells even after 15 min of incubation. It was only after 30 min when weak fluorescence signals were detected for the solid silica nanoparticles and conventional mesoporous silica nanoparticles. It revealed that the unique virus-like mesoporous silica nanoparticles exhibited the fastest internalization rate among the three types of the silica nanoparticles, and they showed powerful signals after incubation for only 5 min. The relative cellular uptake rates were further confirmed by quantification analysis of intracellular nanoparticles. As shown in Figure S17, the uniform virus-like mesoporous silica nanoparticles displayed dramatically higher uptake level than the solid silica nanoparticles and conventional mesoporous silica nanoparticles. The results clearly demonstrated that the virus-like mesoporous silica nanoparticles could enter living cells in large quantities. To exclude the effect of size, aggregation-state, and zeta-potential of the nanoparticles on their cellular uptake property, all these factors above were well controlled to be similar. Dynamic light scattering, zeta-potential, and TEM measurements were carried out, showing a similar size distribution, good monodispersity, and excellent stability (Figures S18–S20). Therefore, the difference in cellular uptake property for the three types of nanomaterials results mainly from the surface morphology (Figure 4a).

To explore the internalization pathways, the three types of the silica nanoparticles were treated with cells in the presence of endocytic inhibitors including chlorpromazine, genistein, and amiloride, respectively. These inhibitors significantly decreased the uptake of the nanoparticles, suggesting the involvement of clathrin-mediated endocytosis, caveolae-mediated endocytosis, and macropinocytosis.[39−41] As shown in Figure S21, the cellular uptake of the uniform virus-like mesoporous silica particles was prohibited to a much smaller degree compared with the two other silica nanoparticles in the presence of chlorpromazine, and to a larger degree in the presence of genistein and amiloride. These results indicated that a larger proportion of the virus-like silica nanoparticles utilized caveolae-mediated endocytosis and macropinocytosis for cellular internalization than the other two nanoparticles. In other words, our unique virus-like mesoporous silica nanoparticles could enter cells with a different strategy compared with the conventional mesoporous silica nanoparticles. The clathrin-mediated pathway may bring about problems in efficient drug delivery as a result of low pH and normal lysosomal degradation.[39,42] The virus-like mesoporous silica nanoparticles can effectively prevent this problem by employing more of the other two pathways. As a result, the virus-like mesoporous silica particles with unique cell internalization pathways are promising drug carriers for a variety of complex conditions.

The virus-like mesoporous silica nanoparticles are also expected to be applicable nanocarriers for drug delivery. The cytotoxicity assay showed that the viability of the cells were over 90% even at a high concentration (~500 μg/mL), indicating good biocompatibility (Figure S22a−c). We also assessed the hemocompatibility of the virus-like mesoporous silica nanoparticles and compared with that for the solid silica and conventional mesoporous silica nanoparticles (Figure S22d). The results show that the virus-like mesoporous silica nanoparticles have a low hemolytic activity. The DOX-loaded conventional and virus-like mesoporous silica nanoparticles had similar release kinetics and proportions at pH 5 and 7 (Figures S23 and S24). The DOX-loaded virus-like mesoporous silica nanoparticles exhibited much higher cytotoxicity than the conventional mesoporous silica nanoparticles (Figure S25), which could be ascribed to the enhanced cellular uptake (with similar loading capacities 28.1 and 27.9 mg/g for the conventional mesoporous silica nanoparticles and virus-like mesoporous silica nanoparticles, respectively).

Persistent blood circulation is especially important in the application of therapeutic nanomedicines.[43,44] The in vivo blood circulation for the three types of silica nanoparticles was studied after intravenous injection into mice (Figure 4c,d). Interestingly, the elimination half-life ($t_{1/2}$) of the virus-like mesoporous silica nanoparticles (2.16 h) was significantly longer than that of the conventional mesoporous silica nanoparticles (0.45 h). This may result from the special surface morphology and good stability in serum conditions (Figure S26), which is consistent with previous reports.[45] Nanocarriers display different biological properties in vitro and in vivo, respectively.[46] It has been reported that nanocarriers exposed to serum may exhibit different biological outcomes from those in the absence of serum, due to the protein layer (corona) that forms on their surface once getting in contact with serum, mediating the interactions with cells.[47] Here, the macrophage endocytosis of conventional and virus-like mesoporous silica nanoparticles was studied in serum-free condition and serum condition, respectively. As shown in Figure S27, strong internalization of both conventional and virus-like mesoporous silica nanoparticles into RAW264.7 cells was observed after incubation in serum-free conditions for 4 h. In contrast, only weak fluorescence signals were detected for the virus-like mesoporous silica nanoparticles in serum conditions after incubation with RAW264.7 for 4 h. Moreover, the quantification analysis of corresponding intracellular nanoparticles further confirmed that macrophages phagocytosis performances of virus-like mesoporous silica nanoparticles were quite different in serum-free and serum conditions (Figure S28). But interestingly, the relatively reduced uptake of virus-like mesoporous silica nanoparticles in serum conditions do not apply to HeLa cells (Figure S29). All these results demonstrate that virus-like mesoporous silica nanoparticles can effectively escape the uptake of macrophage and reduce the immune clearance.

Our strategy of the mesochannel epitaxial growth under an ultralow-surfactant concentration also showed great versatility and could be used to prepare the unique virus-like mesoporous core−shell structures (Figure 5a). The low surfactant concentration biphase system can be applied to coat the surface of core particles of various morphologies and compositions. Magnetic Fe_3O_4 nanoparticles, Ag nanocubes,

DOI: 10.1021/acscentsci.7b00257
ACS Cent. Sci. 2017, 3, 839−846

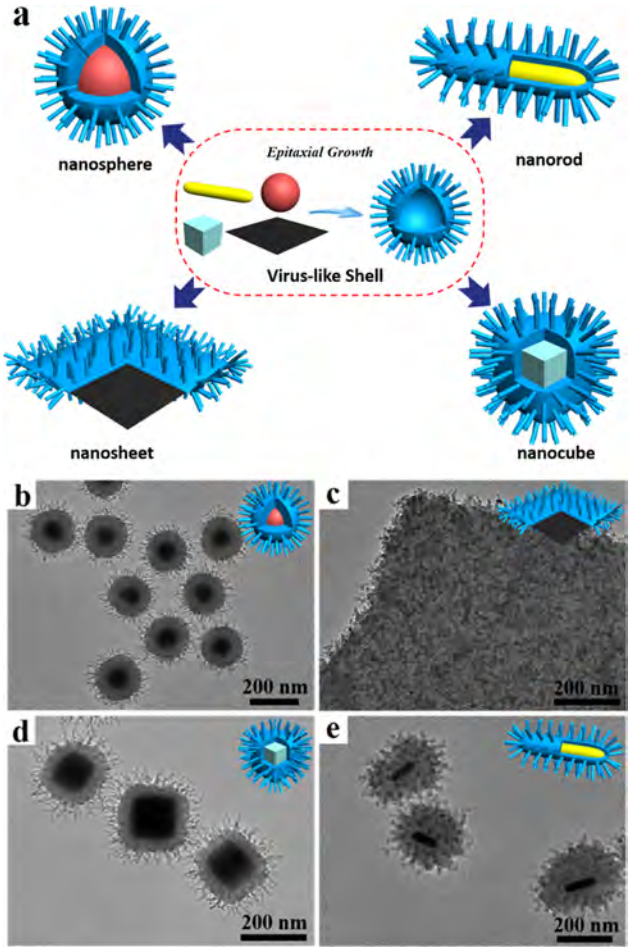

Figure 5. Growth of virus-like mesoporous silica surface on various substrates. (a) Schematic illustration of the growth of virus-like mesoporous silica surface on various substrates. (b–e) TEM images of (b) Fe_3O_4@SiO_2, (c) GO@SiO_2, (d) Ag@SiO_2, and (e) Au@SiO_2 virus-like mesoporous core–shell structures.

Au nanorods, and graphene oxide (GO) nanosheets (Figure S30) were chosen as core particles to demonstrate the feasibility and versatility of our epitaxial growth strategy. In this process, the outer surface of core particles forms a thin silica shell, on which the growth of mesoporous silica shell and virus-like tubes is same as those aforementioned. Fe_3O_4@virus-like silica, Ag@virus-like silica, Au@virus-like silica, and GO@virus-like silica core–shell structures with conformal virus-like mesoporous silica shells could be obtained via the mesochannel epitaxial growth strategy (Figure 5b–e). Our strategy is promising for the fabrication of unique virus-like nanocomposites with various functional cores and rough mesoporous silica shells for diverse applications.

In summary, monodispersed virus-like mesoporous silica nanoparticles constituted by inner nanospheres and peripheral perpendicular nanotubes have successfully been synthesized for the first time on the basis of the single-micelle templating epitaxial growth approach. The obtained virus-like mesoporous silica nanoparticles display very uniform particle size (80–200 nm in diameter) and excellent monodispersity. The peripheral vertically distributed silica nanotubes with an outside/inside diameter of 10/2.5 nm and controllable length (6–70 nm) build up a rough virus-like surface. The formation process of the virus-like silica nanoparticles experiences an isotropic growth of the spherical mesoporous silica nanoparticles followed by an epitaxial growth of the silica nanotubes. The spiky silica nanotubes mainly grow from a portion of the mesochannels of the previously formed mesoporous nanospheres via an epitaxial growth process, creating a rough structure mimicking the spike proteins of a virus. The distance between two adjacent nanotubes is about 30 nm, suggesting that only a few of the mesochannels can grow epitaxially from the necks to form separated long spiky nanotubes. Taking advantage of the virus-like rough surface, the mesoporous silica nanoparticles show a much faster cellular uptake rate compared to the solid and conventional mesoporous silica nanoparticles. The virus-like mesoporous silica nanoparticles loaded with doxorubicin show much higher cancer cell killing efficiency (42%) compared to conventional mesoporous silica nanoparticles (28%), suggesting excellent drug delivery performance due to their unique virus-like structure. In addition, the virus-like silica nanoparticles exhibit unique internalization pathways and extended blood circulation duration. Moreover, our epitaxial growth strategy can be extended to the synthesis of functional nanoparticles@virus-like mesoporous silica core–shell structures, introducing in a virus-like rough surface with mesopore channels and epitaxial spiky nanotubes. Our method can pave the way toward designed synthesis of virus-like structures with various morphologies and compositions for wide applications.

■ ASSOCIATED CONTENT

Supporting Information

The Supporting Information is available free of charge on the ACS Publications website at DOI: 10.1021/acscentsci.7b00257.

Experimental materials, detailed procedures for synthesis, more characterization data, including nitrogen adsorption–desorption isotherms, TEM images, SEM images, SAXS patterns, dynamic light scattering (DLS), and zeta potential, UV–visible absorption spectra, cellular uptake and in vivo blood circulation (PDF)

■ AUTHOR INFORMATION

Corresponding Authors

*(D.Z.) E-mail: dyzhao@fudan.edu.cn.
*(F.Z.) E-mail: zhang_fan@fudan.edu.cn.

ORCID

Fan Zhang: 0000-0001-7886-6144
Dongyuan Zhao: 0000-0001-8440-6902

Notes

The authors declare no competing financial interest.

■ ACKNOWLEDGMENTS

The work was supported by China National Key Basic Research Program (973 Project) (Nos. 2013CB934100 and 2012CB224805), NSFC (Grant Nos. 21322508 and 21210004), Shanghai Shuguang Program, China Postdoctoral Science Foundation (2015M570327). The authors extend their appreciation to the International Scientific Partnership Program ISPP at King Saud University for funding this research work through ISPP# 0018.

■ REFERENCES

(1) Mura, S.; Nicolas, J.; Couvreur, P. Stimuli-responsive nanocarriers for drug delivery. *Nat. Mater.* **2013**, *12*, 991–1003.

DOI: 10.1021/acscentsci.7b00257
ACS Cent. Sci. 2017, 3, 839–846

(2) Gao, X.; Cui, Y.; Levenson, R. M.; Chung, L. W. K.; Nie, S. In vivo cancer targeting and imaging with semiconductor quantum dots. *Nat. Biotechnol.* **2004**, *22*, 969−976.
(3) Peer, D.; Karp, J. M.; Hong, S.; Farokhzad, O. C.; Margalit, R.; Langer, R. Nanocarriers as an emerging platform for cancer therapy. *Nat. Nanotechnol.* **2007**, *2*, 751−760.
(4) Guan, B.; Yu, L.; Lou, X. Formation of Asymmetric Bowl-Like Mesoporous Particles via Emulsion-Induced Interface Anisotropic Assembly. *J. Am. Chem. Soc.* **2016**, *138*, 11306−11311.
(5) Li, Z.; Barnes, J. C.; Bosoy, A.; Stoddart, J. F.; Zink, J. I. Mesoporous silica nanoparticles in biomedical applications. *Chem. Soc. Rev.* **2012**, *41*, 2590−2605.
(6) Petros, R. A.; DeSimone, J. M. Strategies in the design of nanoparticles for therapeutic applications. *Nat. Rev. Drug Discovery* **2010**, *9*, 615−627.
(7) Stark, W. J. Nanoparticles in Biological Systems. *Angew. Chem., Int. Ed.* **2011**, *50*, 1242−1258.
(8) Gao, J.; Gu, H.; Xu, B. Multifunctional Magnetic Nanoparticles: Design, Synthesis, and Biomedical Applications. *Acc. Chem. Res.* **2009**, *42*, 1097−1107.
(9) Xia, F.; Jiang, L. Bio-inspired, smart, multiscale interfacial materials. *Adv. Mater.* **2008**, *20*, 2842−2858.
(10) Niu, Y.; Yu, M.; Hartono, S. B.; Yang, J.; Xu, H.; Zhang, H.; Zhang, J.; Zou, J.; Dexter, A.; Gu, W.; Yu, C. Nanoparticles Mimicking Viral Surface Topography for Enhanced Cellular Delivery. *Adv. Mater.* **2013**, *25*, 6233−6237.
(11) Zhang, Z.; Zhang, X.; Xu, X.; Li, Y.; Li, Y.; Zhong, D.; He, Y.; Gu, Z. Virus-Inspired Mimics Based on Dendritic Lipopeptides for Efficient Tumor-Specific Infection and Systemic Drug Delivery. *Adv. Funct. Mater.* **2015**, *25*, 5250−5260.
(12) Xia, T.; Kovochich, M.; Liong, M.; Meng, H.; Kabehie, S.; George, S.; Zink, J. I.; Nel, A. E. Polyethyleneimine Coating Enhances the Cellular Uptake of Mesoporous Silica Nanoparticles and Allows Safe Delivery of siRNA and DNA Constructs. *ACS Nano* **2009**, *3*, 3273−3286.
(13) Lin, J.; Zhang, H.; Chen, Z.; Zheng, Y. Penetration of Lipid Membranes by Gold Nanoparticles: Insights into Cellular Uptake, Cytotoxicity, and Their Relationship. *ACS Nano* **2010**, *4*, 5421−5429.
(14) Jin, H.; Heller, D. A.; Sharma, R.; Strano, M. S. Size-Dependent Cellular Uptake and Expulsion of Single-Walled Carbon Nanotubes: Single Particle Tracking and a Generic Uptake Model for Nanoparticles. *ACS Nano* **2009**, *3*, 149−158.
(15) Kievit, F. M.; Zhang, M. Surface Engineering of Iron Oxide Nanoparticles for Targeted Cancer Therapy. *Acc. Chem. Res.* **2011**, *44*, 853−862.
(16) Ni, D.; Zhang, J.; Bu, W.; Xing, H.; Han, F.; Xiao, Q.; Yao, Z.; Chen, F.; He, Q.; Liu, J.; Zhang, S.; Fan, W.; Zhou, L.; Peng, W.; Shi, J. Dual-Targeting Upconversion Nanoprobes across the Blood−Brain Barrier for Magnetic Resonance/Fluorescence Imaging of Intracranial Glioblastoma. *ACS Nano* **2014**, *8*, 1231−1242.
(17) Nel, A. E.; Madler, L.; Velegol, D.; Xia, T.; Hoek, E. M. V.; Somasundaran, P.; Klaessig, F.; Castranova, V.; Thompson, M. Understanding biophysicochemical interactions at the nano-bio interface. *Nat. Mater.* **2009**, *8*, 543−557.
(18) Duan, X.; Li, Y. Physicochemical Characteristics of Nanoparticles Affect Circulation, Biodistribution, Cellular Internalization, and Trafficking. *Small* **2013**, *9*, 1521−1532.
(19) Schöttler, S.; Becker, G.; Winzen, S.; Steinbach, T.; Mohr, K.; Landfester, K.; Mailänder, V.; Wurm, F. R. Protein adsorption is required for stealth effect of poly(ethylene glycol)- and poly(phosphoester)-coated nanocarriers. *Nat. Nanotechnol.* **2016**, *11*, 372−377.
(20) Welsher, K.; Yang, H. Multi-resolution 3D visualization of the early stages of cellular uptake of peptide-coated nanoparticles. *Nat. Nanotechnol.* **2014**, *9*, 198−203.
(21) Yang, K.; Ma, Y.-Q. Computer simulation of the translocation of nanoparticles with different shapes across a lipid bilayer. *Nat. Nanotechnol.* **2010**, *5*, 579−583.
(22) Jiang, W.; Kim, B. Y. S.; Rutka, J. T.; Chan, W. C. W. Nanoparticle-mediated cellular response is size-dependent. *Nat. Nanotechnol.* **2008**, *3*, 145−150.
(23) Agarwal, R.; Singh, V.; Jurney, P.; Shi, L.; Sreenivasan, S. V.; Roy, K. Mammalian cells preferentially internalize hydrogel nanodiscs over nanorods and use shape-specific uptake mechanisms. *Proc. Natl. Acad. Sci. U. S. A.* **2013**, *110*, 17247−17252.
(24) Zhang, J.; Yuan, Z.-F.; Wang, Y.; Chen, W.-H.; Luo, G.-F.; Cheng, S.-X.; Zhuo, R.-X.; Zhang, X.-Z. Multifunctional Envelope-Type Mesoporous Silica Nanoparticles for Tumor-Triggered Targeting Drug Delivery. *J. Am. Chem. Soc.* **2013**, *135*, 5068−5073.
(25) Walkey, C. D.; Chan, W. C. W. Understanding and controlling the interaction of nanomaterials with proteins in a physiological environment. *Chem. Soc. Rev.* **2012**, *41*, 2780−2799.
(26) Han, H.-S.; Martin, J. D.; Lee, J.; Harris, D. K.; Fukumura, D.; Jain, R. K.; Bawendi, M. Spatial Charge Configuration Regulates Nanoparticle Transport and Binding Behavior In Vivo. *Angew. Chem., Int. Ed.* **2013**, *52*, 1414−1419.
(27) Zhang, S.; Li, J.; Lykotrafitis, G.; Bao, G.; Suresh, S. Size-Dependent Endocytosis of Nanoparticles. *Adv. Mater.* **2009**, *21*, 419−424.
(28) Albanese, A.; Chan, W. C. W. Effect of Gold Nanoparticle Aggregation on Cell Uptake and Toxicity. *ACS Nano* **2011**, *5*, 5478−5489.
(29) Rancan, F.; Gao, Q.; Graf, C.; Troppens, S.; Hadam, S.; Hackbarth, S.; Kembuan, C.; Blume-Peytavi, U.; Rühl, E.; Lademann, J.; Vogt, A. Skin Penetration and Cellular Uptake of Amorphous Silica Nanoparticles with Variable Size, Surface Functionalization, and Colloidal Stability. *ACS Nano* **2012**, *6*, 6829−6842.
(30) Song, H.; Ahmad Nor, Y.; Yu, M.; Yang, Y.; Zhang, J.; Zhang, H.; Xu, C.; Mitter, N.; Yu, C. Silica Nanopollens Enhance Adhesion for Long-Term Bacterial Inhibition. *J. Am. Chem. Soc.* **2016**, *138*, 6455−6462.
(31) Ahmad Nor, Y.; Niu, Y.; Karmakar, S.; Zhou, L.; Xu, C.; Zhang, J.; Zhang, H.; Yu, M.; Mahony, D.; Mitter, N.; Cooper, M. A.; Yu, C. Shaping Nanoparticles with Hydrophilic Compositions and Hydrophobic Properties as Nanocarriers for Antibiotic Delivery. *ACS Cent. Sci.* **2015**, *1*, 328−334.
(32) Zhu, P.; Liu, J.; Bess, J.; Chertova, E.; Lifson, J. D.; Grisé, H.; Ofek, G. A.; Taylor, K. A.; Roux, K. H. Distribution and three-dimensional structure of AIDS virus envelope spikes. *Nature* **2006**, *441*, 847−852.
(33) Sougrat, R.; Bartesaghi, A.; Lifson, J. D.; Bennett, A. E.; Bess, J. W.; Zabransky, D. J.; Subramaniam, S. Electron Tomography of the Contact between T Cells and SIV/HIV-1: Implications for Viral Entry. *PLoS Pathog.* **2007**, *3*, e63.
(34) Xu, C.; Niu, Y.; Popat, A.; Jambhrunkar, S.; Karmakar, S.; Yu, C. Rod-like mesoporous silica nanoparticles with rough surfaces for enhanced cellular delivery. *J. Mater. Chem. B* **2014**, *2*, 253−256.
(35) Beck, J. S.; Vartuli, J. C.; Roth, W. J.; Leonowicz, M. E.; Kresge, C. T.; Schmitt, K. D.; Chu, C. T. W.; Olson, D. H.; Sheppard, E. W.; McCullen, S. B.; Higgins, J. B.; Schlenker, J. L. A new family of mesoporous molecular sieves prepared with liquid crystal templates. *J. Am. Chem. Soc.* **1992**, *114*, 10834−10843.
(36) Kresge, C. T.; Leonowicz, M. E.; Roth, W. J.; Vartuli, J. C.; Beck, J. S. Ordered mesoporous molecular sieves synthesized by a liquid-crystal template mechanism. *Nature* **1992**, *359*, 710−712.
(37) Polshettiwar, V.; Cha, D.; Zhang, X.; Basset, J. M. High-Surface-Area Silica Nanospheres (KCC-1) with a Fibrous Morphology. *Angew. Chem., Int. Ed.* **2010**, *49*, 9652−9656.
(38) Shen, D. K.; Yang, J. P.; Li, X. M.; Zhou, L.; Zhang, R. Y.; Li, W.; Chen, L.; Wang, R.; Zhang, F.; Zhao, D. Y. Biphase Stratification Approach to Three-Dimensional Dendritic Biodegradable Mesoporous Silica Nanospheres. *Nano Lett.* **2014**, *14*, 923−932.
(39) Conner, S. D.; Schmid, S. L. Regulated portals of entry into the cell. *Nature* **2003**, *422*, 37−44.
(40) Yu, B.; Tang, C.; Yin, C. Enhanced antitumor efficacy of folate modified amphiphilic nanoparticles through co-delivery of chemotherapeutic drugs and genes. *Biomaterials* **2014**, *35*, 6369−6378.

DOI: 10.1021/acscentsci.7b00257
ACS Cent. Sci. 2017, 3, 839−846

(41) He, C.; Yin, L.; Tang, C.; Yin, C. Multifunctional polymeric nanoparticles for oral delivery of TNF-α siRNA to macrophages. *Biomaterials* **2013**, *34*, 2843−2854.
(42) Bareford, L. M.; Swaan, P. W. Endocytic mechanisms for targeted drug delivery. *Adv. Drug Delivery Rev.* **2007**, *59*, 748−758.
(43) Prencipe, G.; Tabakman, S. M.; Welsher, K.; Liu, Z.; Goodwin, A. P.; Zhang, L.; Henry, J.; Dai, H. Branched Polymer for Functionalization of Nanomaterials with Ultralong Blood Circulation. *J. Am. Chem. Soc.* **2009**, *131*, 4783−4787.
(44) Chen, Y.; Chen, H.; Shi, J. In Vivo Bio-Safety Evaluations and Diagnostic/Therapeutic Applications of Chemically Designed Mesoporous Silica Nanoparticles. *Adv. Mater.* **2013**, *25*, 3144−3176.
(45) Hu, X.; Hu, J.; Tian, J.; Ge, Z.; Zhang, G.; Luo, K.; Liu, S. Polyprodrug Amphiphiles: Hierarchical Assemblies for Shape-Regulated Cellular Internalization, Trafficking, and Drug Delivery. *J. Am. Chem. Soc.* **2013**, *135*, 17617−17629.
(46) Schöttler, S.; Becker, G.; Winzen, S.; Steinbach, T.; Mohr, K.; Landfester, K.; Mailänder, V.; Wurm, F. R. Protein adsorption is required for stealth effect of poly (ethylene glycol)-and poly (phosphoester)-coated nanocarriers. *Nat. Nanotechnol.* **2016**, *11*, 372−377.
(47) Lesniak, A.; Fenaroli, F.; Monopoli, M. P.; Å berg, C.; Dawson, K. A.; Salvati, A. Effects of the Presence or Absence of a Protein Corona on Silica Nanoparticle Uptake and Impact on Cells. *ACS Nano* **2012**, *6*, 5845−5857.

DOI: 10.1021/acscentsci.7b00257
ACS Cent. Sci. 2017, 3, 839−846